Research Article

Structural, morphological and cryogenic magnetic behaviour of double perovskite $La_{1.9}Sr_{0.1}NiMnO_{6-\delta}$ thin film

Shah Aarif Ul Islam[1] · Khalid Sultan[2] · Sheeraz Ahmad Bhat[1] · Nazima Nazir[1] · Mohd Ikram[1]

Received: 28 January 2020 / Accepted: 14 March 2020 / Published online: 20 March 2020

Abstract
This work presents the investigation on structural, morphological and cryogenic/temperature-dependent magnetic studies carried on the hole-doped double perovskite $La_{1.9}Sr0_{0.1}NiMnO_{6-\delta}$ thin film. The optimized film was deposited on Si (100) substrate through pulsed laser ablation. The film was characterized by the techniques, grazing incidence X-ray diffraction (GIXRD), atomic force microscopy (AFM), Raman and temperature-dependent magnetization. GIXRD patterns revealed the polycrystalline structure to be monoclinic and possessing $P2_1/n$ space group. The tensile strain was detected in the film and estimated from the Williamson-Hall equation. AFM micrographs revealed the average grain size and the film roughness. Raman peaks corresponding to the wavenumbers 530 cm^{-1} and 657 cm^{-1}, respectively represent the asymmetric and symmetric modes of the NiO_6/MnO_6 octahedra. Besides, magnetic studies revealed the ferromagnetic nature of the film at cryogenic temperature (5 K) as depicted by the MH loop along with the curie temperature of 186.9 K was obtained from the MT plots.

Keywords Thin film · PLD · AFM · Magnetization · Curie temperature

1 Introduction

Perovskite oxides of general formula $A_2BB'O_6$, where A site is occupied by rare-earth or an alkaline earth cation, B and B′ sites occupied by transition metals are called as double perovskites [1]. These oxides have been known from many decades, while the first studies on these compounds have initiated in about 1950s. Since then hundreds of compounds belonging to this family have been synthesized and studied as they display interesting and diverse structural, magnetic and electronic properties [2]. The practical diversity in the physical properties exhibited by these compounds is because of the fact that there is considerable scope for formation of new compounds by just choosing the A site, B and B′ site ions among the alkaline earth metals/ rare earth and transition metals respectively. Physical properties exhibited by the double perovskites are mostly determined by the B and B′ transition metal cations. In last many years, there has been a surge of interest in the synthesis and studies on the double perovskite oxides as some of the compounds belonging to this family like Sr_2FeMoO_6, La_2VRuO_6, La_2NiMnO_6, Gd_2NiMnO_6, La_2CoMnO_6 etc. display remarkable physical properties such as colossal magnetoresistance, half-metallicity, ferromagnetism etc. [3, 4]. The other technologically important applications exhibited by these double perovskites include solid-state Peltier coolers [5], magnetodielectric capacitors [6, 7], spintronic devices [8–12] tunnel junctions [13, 14] and most importantly solar cell applications [15]. Due to these versatile properties and potential applications, these oxides figure among the most investigated compounds by the researchers.

✉ Shah Aarif Ul Islam, aarifulislam111@gmail.com | [1]Solid State Research Laboratory, Department of Physics, National Institute of Technology, Srinagar, J&K 190006, India. [2]Department of Physics, Central University of Kashmir, Tullamullah, Ganderbal, J&K 190015, India.

Out of this family of double perovskites, the manganite oxides R_2MMnO_6, where M = (Ni, Co) by virtue of being ferromagnetic semiconductors and possessing vast magnetic and electronic properties [9, 10, 16–20] are of highest interest. Particularly, La_2NiMnO_6, having potential applications in spintronics [10, 21] has grabbed more focus. Also, the fundamental laws governing the physical properties of La_2NiMnO_6 are interesting [22, 23], since most of these oxides are antiferromagnetic owing to super-exchange interactions, however, is ferromagnetic. The magnetic properties being governed by Kanamori & Goodenough rules [24] wherein the ordered arrangement of MnO_6 & NiO_6 octahedra leads to ferromagnetic interactions between Mn^{4+} and Ni^{2+}cations. Thus, this oxide possesses remarkable ferromagnetic properties. Besides, significant changes are possible in the physical properties of La_2NiMnO_6 when some suitable dopant is added at the La site [25]. The doping in La_2NiMnO_6 compounds carries a great significance owing to the applications especially in magnetoresistance, solar cells and spintronics [15, 26–29]. The studies on the bulk as well as thin films of La_2NiMnO_6 has attracted a lot of research because of its applications in solar cells [15], spintronic devices, magnetic memory devices [10, 29–35], photovoltaic cells [36] and hydrogen storage [37]. Not enough work has yet been performed on the thin films of La_2NiMnO_6 though the studies on bulk have been many. Thin films of La_2NiMnO_6 are commonly deposited by chemical solution deposition [38] or pulsed laser deposition [33, 39]. The deposition parameters, however, play a crucial part in defining the properties of the deposited films. Therefore, to achieve better properties, it is imperative to deposit the films in optimized circumstances. The optimized film fabrication besides doping is therefore highly important for the device applications.

This work presents the optimized fabrication of $La_{1.9}Sr_{0.1}NiMnO_{6-\delta}$ thin film on the substrate of Si (1 0 0) synthesized by pulsed laser deposition. This technique was chosen as it precisely retains the target-stoichiometry on the substrate. Sr was substituted at the La site as a dopant. Mainly the structure analysis, morphology and the magnetic studies performed on $La_{1.9}Sr_{0.1}NiMnO_{6-\delta}$ are explained in this manuscript and the parameters of interest like structural phase, grain size, roughness and magnetic parameters including coercivity, remanence, Curie temperature etc. are discussed.

2 Experimental details

The thin film of $La_{1.9}Sr_{0.1}NiMnO_{6-\delta}$ (hereafter referred to as LSNMO) was deposited by pulsed laser deposition (PLD) technique. A fine powder of LSNMO, prepared by the solid-state reaction was hydraulically pelletized and made into pellets of 15 mm diameter and 2 mm thickness. This pellet was used as the target for the deposition of a thin film of LSNMO on Si (1 0 0) substrate. Before the start of deposition, the substrate was cleaned with an ultrasonic bath in acetone and the deposition chamber was cleaned by using ethanol. The target was placed on the target holder and the substrate was placed on the substrate holder. Both of them were aligned with each other and separated by a distance of 40 mm. Later the heating was started and the substrate temperature was raised to 700-degree centigrade. The chamber was filled with 99.8% pure oxygen and the deposition was done against the oxygen background pressure of 500 mTorr. Lambda-Physik LPX210 an excimer laser source having a wavelength of 248 nm was used for the deposition. The laser source of incident energy 270 mJ was focussed on the target and the deposition was started and lasted for 40 min at a frequency of 10 pulses per second. This incident laser ablated the material from the target and the stoichiometric ablated material was deposited on the substrate kept at a temperature of 700 degrees. After finishing deposition, the substrate temperature was decreased to 550 degrees and the deposited film was annealed for 30 min by filling the chamber with 760 mTorr oxygen. Afterwards, the annealed film was cooled at a rate of 10 degrees per minute down to the room temperature and the LSNMO film was taken out.

The phase identification of the as-prepared film was done by performing the grazing incidence X-ray diffraction with a grazing angle of 1°, using the Bruker AXS D8 Discover X-ray diffractometer. The scan was carried out in the 2θ range of 15°–80°. The surface morphology of the film was studied with the help of atomic force microscopy (AFM), using Nanoscope E digital instrument in tapping mode. Renishaw in via microscope having 520 nm as wavelength was used to record the Raman spectra of the film. To avoid any damage to the film the laser power was minimized to 0.3 mW. The magnetic measurements were performed on the 7 T MPMS, SQUID. The MH, hysteresis measurement was done in the field − 3 T to + 3 T at a cryogenic temperature of 5 K. Moreover, the MT, magnetisation versus temperature in ZFC and FC condition was recorded in the temperature ranging from 5 to 300 K in a coercive field of 300 Oe.

3 Results and discussion

3.1 GIXRD analysis

The GIXRD pattern of $La_{1.9}Sr_{0.1}NiMnO_{6-\delta}$ showing the polycrystalline nature of the film is shown in Fig. 1. All the diffraction peaks corresponding to monoclinic phase like (110), (112), (202), (220), (310), (312), (204) and (224) are present

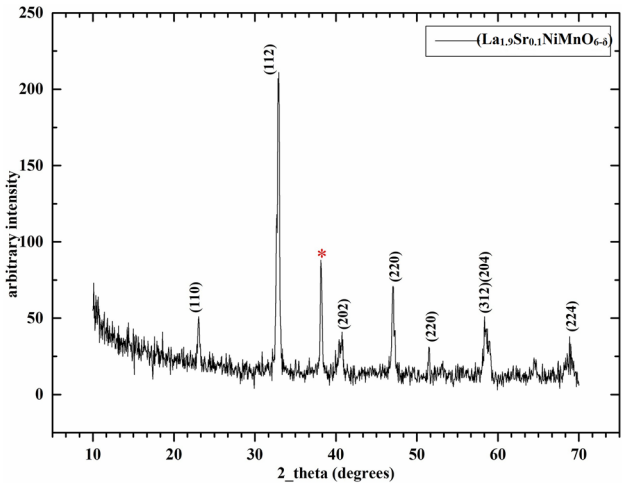

Fig. 1 Grazing incidence XRD pattern of double perovskite $La_{1.9}Sr_{0.1}NiMnO_{6-\delta}$ film

in the film, confirming the single phase that is the monoclinic phase with $P2_1/n$ space group as also reported in bulk La_2NiMnO_6 target [28, 40]. The extra peak around 38 degrees is from the precursor Mn_2O_3 [41] (JCPDS Card No. 78-0390), that might have remained unmixed. The lattice parameters calculated on the basis of the monoclinic structure are presented in Table 1. Scherrer's equation was used to obtain the crystallite size:

$$D = K\lambda/\beta cos\theta$$

In the above equation, D represents the crystallite size, K is a shape factor mostly taken as 0.9, λ, the X-ray wavelength (for CuKα source = 1.54 A°), β, the full width at half maximum intensity for the chosen Bragg peak. The obtained value of the crystallite size from the above equation is presented in Table 1.

The lattice strain present in the film was calculated from the Williamson Hall equation.

$$\beta_{hkl} \cos\theta = {}^{K\lambda}/_{D} + 4\varepsilon \sin\theta$$

Again here (β_{hkl}) is full width at half maximum of a chosen Bragg peak, $K = 0.9$ is a shape factor constant, λ, the source X-ray wavelength, D represents the crystallite size and the term ε in the above equation of Williamson and hall is the magnitude of strain. The term $(\beta_{hkl} \cos\theta)$ along the Y-axis is plotted against $4\varepsilon \sin\theta$ along X-axis. The slope of the linear fit of this plot yields the strain and the intercept on the Y-axis of this linear fit line represents the Crystallite size. The values of strain (ε) and crystallite size (D) calculated by this Williamson hall analysis are reported in Table 1.

3.2 AFM analysis

The morphology, grain diameter and surface roughness of the film $La_{1.9}Sr_{0.1}NiMnO_{6-\delta}$ were studied from the AFM micrographs. The AFM micrographs are shown in Fig. 2. The morphology of the deposited film is more or less spherical with some flattened spherical grains. Different parameters like grain diameter and roughness were calculated from the software Nanoscope. The grain diameter, taken as the root mean square value came around to be 171.41 nm. Also, the roughness was estimated to be about 10.32 nm. The values are reported in Table 2.

3.3 Raman analysis

Figure 3 represents the Raman spectra of $La_{1.9}Sr_{0.1}NiMnO_{6-\delta}$ thin film on Si (1 0 0) taken at room temperature. The spectra show dominant modes at the wavenumbers (530 and 657) cm^{-1}. The intensity and the number of peaks appearing in Raman spectra are closely associated with the deviation from the ideal cubic structure of La_2NiMnO_6.

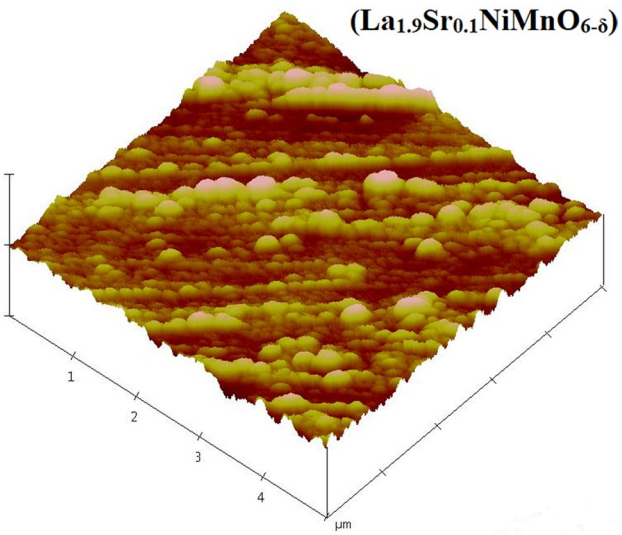

Fig. 2 Surface morphology of $La_{1.9}Sr_{0.1}NiMnO_{6-\delta}$ thin-film represented by AFM images

Table 1 Lattice parameters, crystallite size and value of strain for the $La_{1.9}Sr_{0.1}NiMnO_{6-\delta}$ film

Film composition	a (Å)	b (Å)	c (Å)	FWHM	Crystallite size (D) in (nm)		Strain $\times 10^{-1}$
					Debye–Scherrer	Williamson Hall	
$La_{1.9}Sr_{0.1}NiMnO_6$	5.432	5.481	7.674	0.351	24.162	31.241	1.174

Table 2 The surface roughness, grain size and magnetic parameters of $La_{1.9}Sr_{0.1}NiMnO_{6-\delta}$ film

Film composition	Surface roughness (nm)	Grain diameter (nm)	Hc	Mr	Ms	Tc
$La_{1.9}Sr_{0.1}NiMnO_6$	10.32	171.41	371.13	43.78	57.46	186.90 K

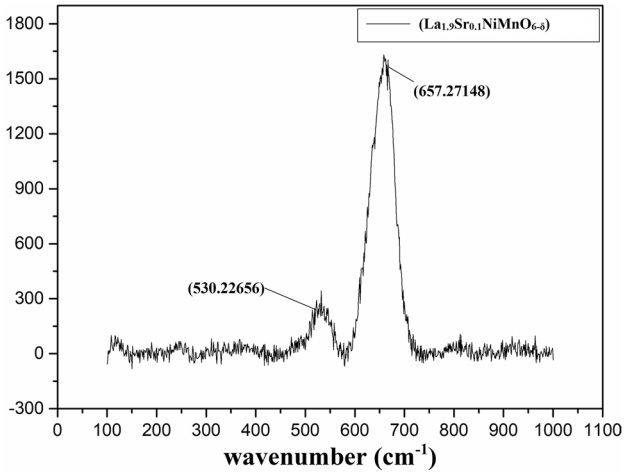

Fig. 3 Raman spectra of $La_{1.9}Sr_{0.1}NiMnO_{6-\delta}$ film showing characteristic symmetric and asymmetric stretching modes

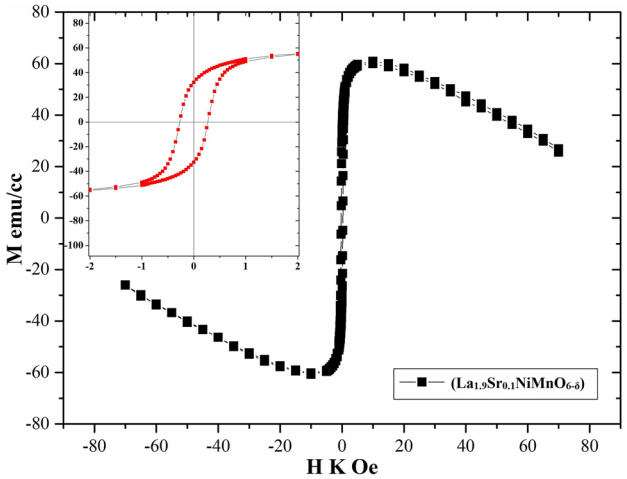

Fig. 4 The MH hysteresis curve of $La_{1.9}Sr_{0.1}NiMnO_{6-\delta}$ thin-film recorded at 5 K. Inset presents the zoomed view to highlight the ferromagnetic loop

These modes respectively correspond to the asymmetrical stretching (AS) and symmetrical stretching (S) of MnO_6/NiO_6 octahedra. Also, these modes are characteristic of the monoclinic structure with space group as $P2_1/n$ [28], accomplishing the Ni/Mn cation ordering and hence consistent with the XRD results [30]. The FWHM of the corresponding Raman peaks is not much broad, which implies that the crystallization of the film is better [42].

3.4 Magnetic study

Figure 4 represents the isothermal, magnetization vs applied field behaviour (MH curve) of $La_{1.9}Sr_{0.1}NiMnO_6$ taken at cryogenic temperature of 5 K. The inset shows the presence of hysteresis loop which is ferromagnetic in nature and having a coercivity (*Hc*) of 371 K. The MH curve was obtained to study the role of magnetic domains giving rise to all the magnetic properties of $La_{1.9}Sr_{0.1}NiMnO_{6-\delta}$ and thus attain the magnetic parameters like, *Hc, Mr and Ms* that is coercivity, remnant magnetization and saturation magnetization respectively. The values of all these parameters are listed in Table 2. The saturated magnetic moment, μ_B/f.u. for the LSNMO/Si (100), at the 5 K temperature has been calculated by the formula [43];

$$\mu_B/f.u. = \left(M_s * M_w\right)/5585$$

where M_s is the maximum value of saturation magnetization and M_w is the molecular weight of the sample in grams. The value came out to be (4.96 μ_B/f.u.), as compared to the value of 4.63 μ_B/f.u. obtained by H Guo et.al [39]. in the epitaxial thin films of La_2NiMnO_6 on $SrTiO_3$ (STO) substrate.

Figure 5 represents the temperature-dependent magnetization that is MT-curve of $La_{1.9}Sr_{0.1}NiMnO_{6-\delta}$ taken within the 5 K to 300 K temperature range. The MT curve has been obtained by the field applied parallel to the film surface with a coercive field/ applied field of 500 Oe. The sample was first cooled in SQUID chamber down to 5 K without applying any external field.

After that zero-field cooled (ZFC), magnetization versus temperature (MT) was taken under a constant coercive magnetic field of 500 Oe. The ZFC-MT was recorded during heating in the temperature range of 5–300 K. Subsequently, field cooled (FC), magnetization versus temperature (MT) was taken under the same constant coercive field. Also, the FC-MT was recorded while cooling the sample in the temperature range of 300–5 K. From the MT curves in Fig. 5, it is clearly seen that the magnetization decreases with the corresponding increase in the temperature. The first derivative of Magnetization with respect to the temperature that is dM/dT was taken and the minima of this curve represents the ferromagnetic curie temperature, T_c. The value of curie temperature was found to be

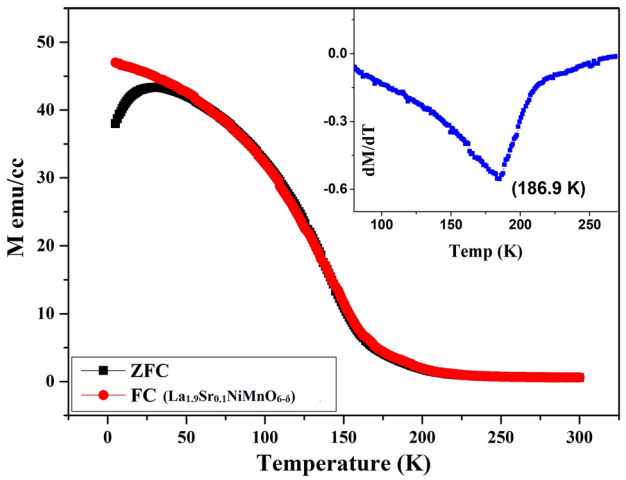

Fig. 5 Field cooled and zero field cooled MT-curves of $La_{1.9}Sr_{0.1}NiMnO_{6-\delta}$ film. Inset presents the value of Tc calculated from the minima of dM/dT

186.9 K. An enhancement in value of T_c is clearly seen from that of the pure LNMO when compared with our previous report [40]. The enhancement in T_c may possibly be due to the change of the valency of Ni from + 2 to + 3 upon Sr doping to maintain charge neutrality in the compound. Moreover, LNMO has been reported to exhibit more than one magnetic transition, largely depending on the synthesis conditions. Two FM transitions at $T_c1 \sim 280$ K and $T_c2 \sim 150$ K have also been reported in some reports [17, 30, 32, 44]. Besides, in MT curves, the point where ZFC and FC curves segregate from each other is called the temperature of irreversibility and may also be called as the magnetic-ordering temperature. The permanent difference at a lower temperature as seen from the MT curves between ZFC and FC curves clearly indicates that the deposited film has well magnetic ordering.

4 Conclusion

Thin-film of $La_{1.9}Sr_{0.1}NiMnO_{6-\delta}$ was successfully deposited from the bulk target on Si (1 0 0) substrate using pulsed laser ablation technique. Polycrystalline nature of the grown film was revealed from the GIXRD patterns. X-ray analysis confirmed the monoclinic structure of the film having $P2_1/n$ space group. The tensile strain was noted in the film and the strain value was calculated from the Williamson-Hall equation. The morphology showed the spherical grains with average grain size and roughness calculated by the Nanoscope software. The asymmetric and symmetric stretching modes of the NiO_6/MnO_6 octahedra were revealed by the wavenumbers corresponding to 530 cm^{-1} and 657 cm^{-1} in the Raman spectra of the film. Moreover, the ferromagnetic nature of the film at a cryogenic temperature of 5 K was revealed from the magnetic studies as depicted by the MH loop. Also, the ferromagnetic curie temperature Tc calculated from the MT plots was found to be 186.9 K for this film.

Acknowledgements The author (KS), would like to thank UGC for financial support under UGC-BSR start-up grant no. F.30–395/2017(BSR). (SAUI), (SAB) & (NN) acknowledge the support from National Institute of Technology, NIT Srinagar.

Compliance with ethical standards

Conflict of interest The authors declare that they have no conflict of interest.

References

1. Flerov IN, Gorev MV, Aleksandrov KS, Tressaud A, Grannec J, Couzi M (1998) Phase transitions in elpasolites (ordered perovskites). Mater Sci Eng R Rep 24(3):81–151
2. Anderson MT, Greenwood KB, Taylor GA, Poeppelmeier KR (1993) B-cation arrangements in double perovskites. Prog Solid State Chem 22(3):197–233
3. Sarma DD (2001) A new class of magnetic materials: Sr_2FeMoO_6 and related compounds. Curr Opin Solid State Mater Sci 5(4):261–268
4. Viola MD, Martinez-Lope MJ, Alonso JA, Velasco P, Martinez JL, Pedregosa JC, Carbonio RE, Fernández-Díaz MT (2002) Induction of colossal magnetoresistance in the double perovskite Sr_2CoMoO_6. Chem Mater 14(2):812–818
5. Fiebig M, Lottermoser T, Fröhlich D, Goltsev AV, Pisarev RV (2002) Observation of coupled magnetic and electric domains. Nature 419(6909):818
6. Kimura T, Kawamoto S, Yamada I, Azuma M, Takano M, Tokura Y (2003) Magnetocapacitance effect in multiferroic $BiMnO_3$. Phys Rev B 67(18):180401
7. Lawes G, Ramirez AP, Varma CM, Subramanian MA (2003) Magnetodielectric effects from spin fluctuations in isostructural ferromagnetic and antiferromagnetic systems. Phys Rev Lett 91(25):257208
8. Kobayashi KI, Kimura T, Sawada H, Terakura K, Tokura Y (1998) Room-temperature magnetoresistance in an oxide material with an ordered double-perovskite structure. Nature 395(6703):677
9. Choudhury D, Mandal P, Mathieu R, Hazarika A, Rajan S, Sundaresan A, Waghmare UV, Knut R, Karis O, Nordblad P, Sarma DD (2012) Near-room-temperature colossal magnetodielectricity and multiglass properties in partially disordered La_2NiMnO_6. Phys Rev Lett 108(12):127201
10. Rogado NS, Li J, Sleight AW, Subramanian MA (2005) Magnetocapacitance and magnetoresistance near room temperature in a ferromagnetic semiconductor: La_2NiMnO_6. Adv Mater 17(18):2225–2227
11. Kuepper K, Kadiroglu M, Postnikov AV, Prince KC, Matteucci M, Galakhov VR, Hesse H, Borstel G, Neumann M (2005) Electronic structure of highly ordered Sr_2FeMoO_6: XPS and XES studies. J Phys Condens Matter 17(27):4309
12. Raekers M, Kuepper K, Hesse H, Balasz I, Deac IG, Constantinescu S, Burzo E, Valeanu M, Neumann M (2006) Investigation of chemical and grain boundary effects in highly ordered Sr_2FeMoO_6: XPS and Mossbauer studies. J Optoelectron Adv Mater 8(2):455

13. Lüders U, Bibes M, Bouzehouane K, Jacquet E, Contour JP, Fusil S, Bobo JF, Fontcuberta J, Barthélémy A, Fert A (2006) Spin filtering through ferrimagnetic $NiFe_2O_4$ tunnel barriers. Appl Phys Lett 88(8):082505
14. Gajek M, Bibes M, Barthélémy A, Bouzehouane K, Fusil S, Varela M, Fontcuberta J, Fert A (2005) Spin filtering through ferromagnetic $BiMnO_3$ tunnel barriers. Phys Rev B 72(2):020406
15. Lan C, Zhao S, Xu T, Ma J, Hayase S, Ma T (2016) Investigation on structures, band gaps, and electronic structures of lead-free La_2NiMnO_6 double perovskite materials for potential application of solar cell. J Alloy Compd 655:208–214
16. Das H, Waghmare UV, Saha-Dasgupta T, Sarma DD (2008) Electronic structure, phonons, and dielectric anomaly in ferromagnetic insulating double perovskite La_2NiMnO_6. Phys Rev Lett 100(18):186402
17. Dass I, Goodenough JB (2003) Multiple magnetic phases of La_2CoMnO_6-δ (0≤ δ ≤ 0.05). Phys Rev B 67(014401):9
18. Nair HS, Swain D, Adiga S, Narayana C, Elzabeth S (2011) Griffiths phase-like behaviour and spin-phonon coupling in double perovskite Tb_2NiMnO_6. J Appl Phys 110(12):123919
19. Singh MP, Truong KD, Jandl S, Fournier P (2011) Magnetic properties and phonon behaviour of Pr_2NiMnO_6 thin films. Appl Phys Lett 98(16):162506
20. Tang MH, Xiao YG, Jiang B, Hou JW, Li JC, He J (2011) The giant dielectric tunability effect in bulk Y_2NiMnO_6 around room temperature. Appl Phys A 105(3):679–683
21. Itoh H, Ozeki J, Inoue J (2007) Electronic structure and spin-filter effect of ferromagnetic insulators with double perovskite structure. J Magn Magn Mater 310(2):1994–1996
22. Wold A, Arnott RJ, Goodenough JB (1958) Some Magnetic and Crystallographic Properties of the System $LaMn_{1-x}Ni_xO_{3+\lambda}$. J Appl Phys 29(3):387–389
23. Blasse G (1965) Ferromagnetic interactions in non-metallic perovskites. J Phys Chem Solids 26(12):1969–1971
24. Goodenough JB (1955) Theory of the role of covalence in the perovskite-type manganites [La, M(II)] MnO_3. Phys Rev 100(2):564
25. Booth RJ, Fillman R, Whitaker H, Nag A, Tiwari RM, Ramanujachary KV, Gopalakrishnan J, Lofland SE (2009) An investigation of structural, magnetic and dielectric properties of R_2NiMnO_6 (R = rare earth, Y). Mater Res Bull 44(7):1559–1564
26. Guo Y, Shi L, Zhou S, Zhao J, Wang C, Liu W, Wei S (2013) Tunable exchange bias effect in Sr-doped double perovskite La_2NiMnO_6. J Phys D Appl Phys 46(17):175302
27. Kim B, Choi HC, Kim BH, Min BI (2010) Electronic structure and magnetic properties of hole-carrier-doped La_2MnNiO_6: $La_{2-x}Sr_xMnNiO_6$. Phys Rev B 81(22):224402
28. Islam SA, Ikram M (2019) Structural stability improvement, Williamson Hall analysis and band-gap tailoring through A-site Sr doping in rare-earth-based double perovskite La_2NiMnO_6. Rare Metals 38(9):805–813
29. Guo HZ, Burgess J, Ada E, Street S, Gupta A, Iliev MN, Kellock AJ, Magen C, Varela M, Pennycook SJ (2008) Influence of defects on structural and magnetic properties of multifunctional La_2NiMnO_6 thin films. Phys Rev B 77(17):174423
30. Bull CL, Gleeson D, Knight KS (2003) Determination of B-site ordering and structural transformations in the mixed transition metal perovskites La_2CoMnO_6 and La_2NiMnO_6. J Phys Condens Matter 15(29):4927
31. Padhan P, Guo HZ, LeClair P, Gupta A (2008) Dielectric relaxation and magnetodielectric response in epitaxial thin films of La_2NiMnO_6. Appl Phys Lett 92(2):022909
32. Singh MP, Grygiel C, Sheets WC, Boullay P, Hervieu M, Prellier W, Mercey B, Simon C, Raveau B (2007) Absence of long-range Ni/Mn ordering in ferromagnetic La_2NiMnO_6 thin films. Appl Phys Lett 91(1):012503
33. Hashisaka M, Kan D, Masuno A, Takano M, Shimakawa Y, Terashima T, Mibu K (2006) Epitaxial growth of ferromagnetic La_2NiMnO_6 with ordered double-perovskite structure. Appl Phys Lett 89(3):032504
34. Iliev MN, Guo H, Gupta A (2007) Raman spectroscopy evidence of strong spin-phonon coupling in epitaxial thin films of the double perovskite La_2NiMnO_6. Appl Phys Lett 90(15):151914
35. Lin YQ, Chen XM, Liu XQ (2009) Relaxor-like dielectric behaviour in La_2NiMnO_6 double perovskite ceramics. Solid State Commun 149(19–20):784–787
36. Sheikh MS, Ghosh D, Dutta A, Bhattacharyya S, Sinha TP (2017) Lead-free double perovskite oxides Ln_2NiMnO_6 (Ln = La, Eu, Dy, Lu), a new promising material for photovoltaic application. Mater Sci Eng B 226:10–17
37. Henao J, Sotelo O, Casales-Diaz M, Martinez-Gomez L (2018) Hydrogen storage in a rare-earth perovskite-type oxide $La_{0.6}Sr_{0.4}Co_{0.2}Fe_{0.8}O_3$ for battery applications. Rare Metals 37(12):1003–13
38. Wang T, Xu W, Fang X, Dong W, Tao R, Li D, Zhao Y, Zhu X (2009) Chemical solution deposition preparation of double-perovskite La_2NiMnO_6 film on $LaAlO_3$ (0 0 1) substrate. J Alloy Compd 475(1–2):9–12
39. Guo H, Burgess J, Street S, Gupta A, Calvarese TG, Subramanian MA (2006) Growth of epitaxial thin films of the ordered double perovskite La_2NiMnO_6 on different substrates. Appl Phys Lett 89(2):022509
40. Islam SAU, Ikram M (2019) Effect of strontium substitution on the structural, morphological and magnetic properties of $La_{2-x}Sr_xNiMnO_6$ double perovskite thin films deposited on Si (100). Mater Res Express 6:096416
41. Zheng H, Wang T, Chen J, Liu Q, Zhao R, Li L (2017) Facile synthesis of porous Mn_2O_3 microsphere as an anode material for lithium ion batteries. In: Materials science and engineering conference series, vol 274, no 1, 2017 Dec, p 012162
42. Wang T, Fang X, Dong W, Tao R, Deng Z, Li D, Zhao Y, Meng G, Zhou S, Zhu X (2008) Fabrication of polycrystalline La_2NiMnO_6 thin films on LaAlO3 (1 0 0) substrates by chemical solution deposition. J Cryst Growth 310(14):3386–3390
43. Kumar G, Shah J, Kotnala RK, Singh VP, Sarveena Garg G, Shirsath SE, Batoo KM, Singh M (2015) Superparamagnetic behaviour and evidence of weakening in super-exchange interactions with the substitution of Gd^{3+} ions in the Mg–Mn nanoferrite matrix. Mater Res Bull 63:216–225
44. Goodenough JB (1976) Magnetism and the chemical bond. Inter Science Publication, New York